Supplemental materials for
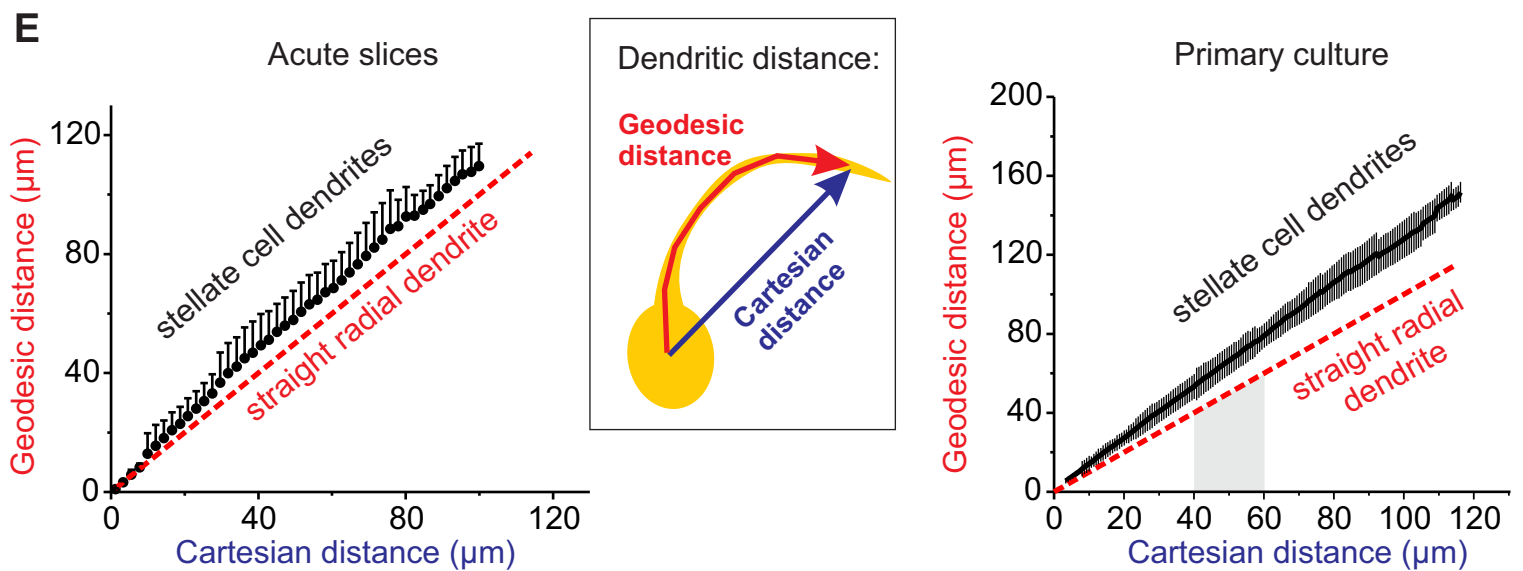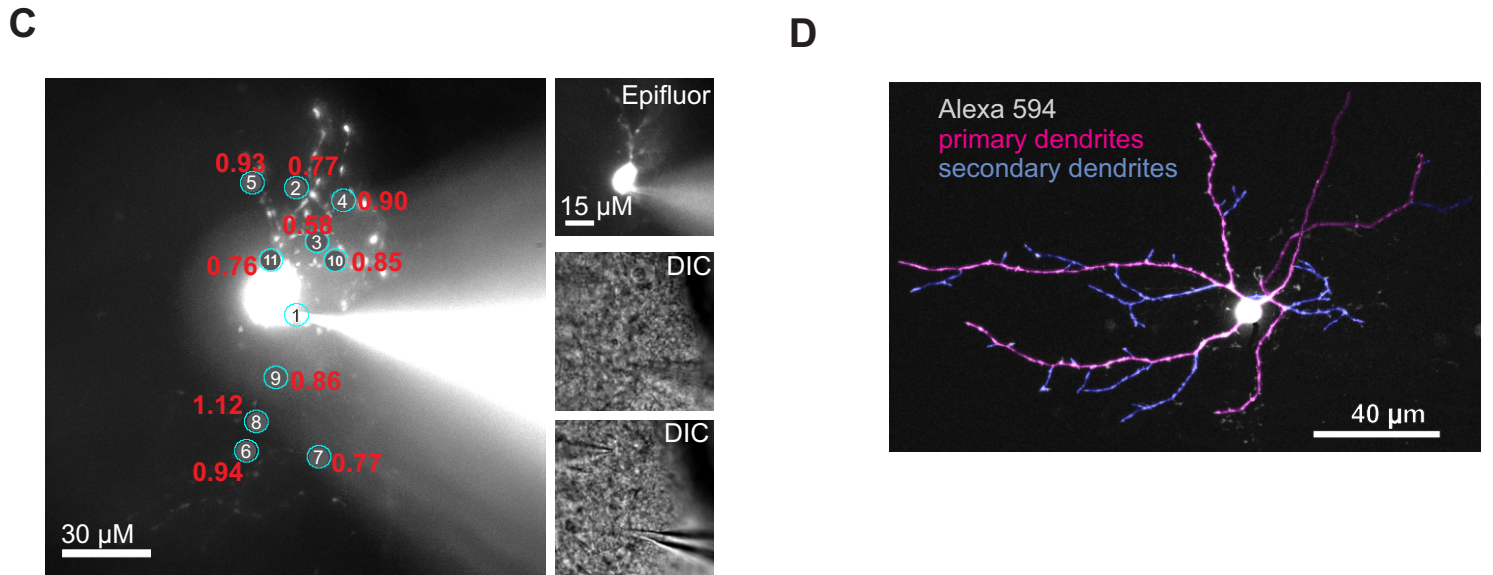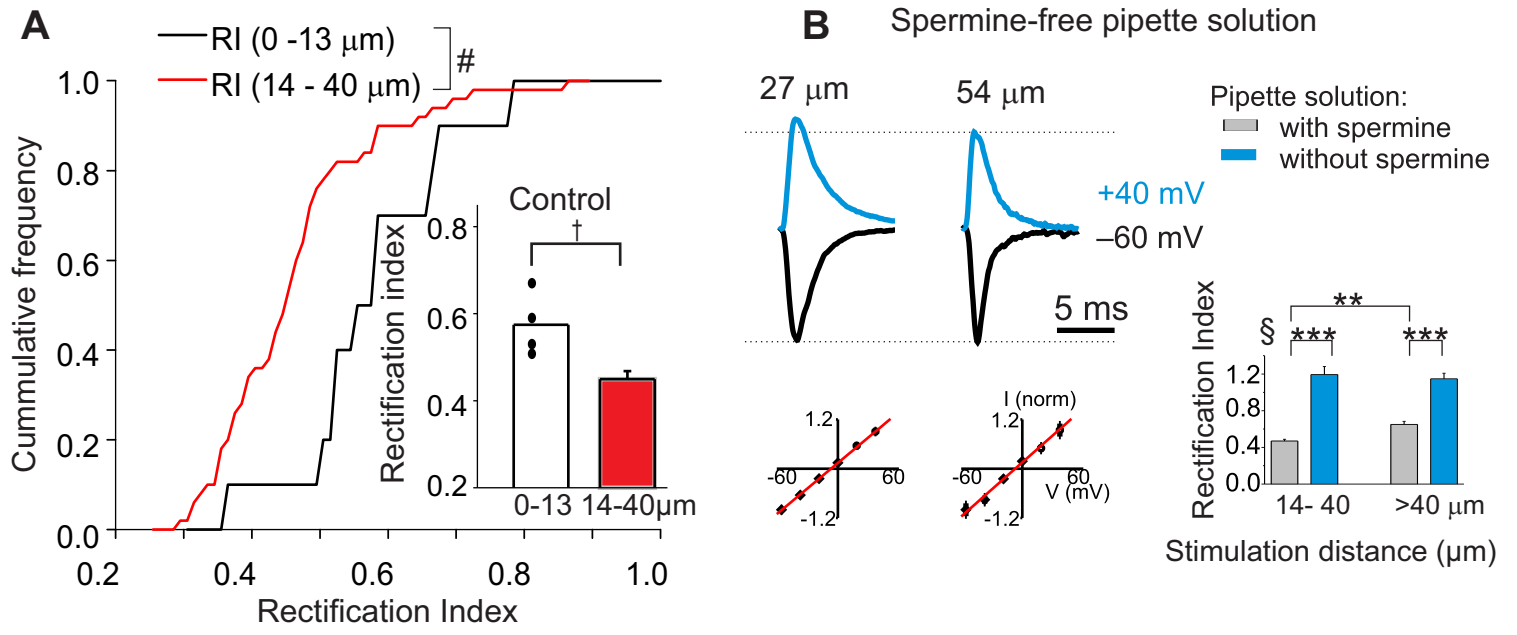
Topological regulation of synaptic AMPA receptor expression by the RNA-binding protein CPEB3

Iaroslav Savtchouk [1,2] *, Lu Sun[1,2]*, Crhistian L. Bender [1,*] Qian Yang[1,*], Gábor Szabó [4], Sonia Gasparini[1,3], and Siqiong June Liu[1,2]

Correspondence to sliu@lsuhsc.edu

This PDF file includes:

    Supplementary Figures S1-S8

    Supplemental Experimental Procedures

    Supplementary References

    Supplemental Table S1

A

RI (0 -13 μm)
RI (14 - 40 μm)

#

Cummulative frequency

1.0
0.8
0.6
0.4
0.2
0.0

0.2   0.4   0.6   0.8   1.0
Rectification Index

Control

Rectification index

†

0.8
0.6
0.4
0.2

0-13   14-40μm

B   Spermine-free pipette solution

27 μm   54 μm

+40 mV
−60 mV

5 ms

Pipette solution:
with spermine
without spermine

1.2   I (norm)   1.2
              1.2
−60   60   −60   60   V (mV)
−1.2   −1.2

Rectification Index

§   **   ***   ***

1.2
0.8
0.4
0.0

14- 40   >40 μm
Stimulation distance (μm)

C

0.93 0.77
⑤   ②
②   ④ 0.90
    0.58
0.76 ③
⑪   ⑩ 0.85
    ①
    ⑨ 0.86
1.12
⑧
0.94 ⑥   ⑦ 0.77

30 μM

Epifluor

15 μM

DIC

DIC

D

Alexa 594
primary dendrites
secondary dendrites

40 μm

E

Acute slices

Geodesic distance (μm)

120
80
40
0

stellate cell dendrites

straight radial dendrite

0   40   80   120
Cartesian distance (μm)

Dendritic distance:

Geodesic
distance

Cartesian
distance

Primary culture

Geodesic distance (μm)

200
160
120
80
40
0

stellate cell dendrites

straight radial
dendrite

0   20   40   60   80   100   120
Cartesian distance (μm)

Supplemental Figure 1. Characterization of EPSC rectification index and dendritic distance, Related to Figure 1**. A**. Rectification index of synaptic AMPARs on the soma *vs* proximal dendrites. Putative somatic synapses are those located within 13 µm from the tip of the recording electrode. The rectification index of putative somatic synapses (0-13 µm) and of synapses onto proximal dendrites (14-40 µm) from control experiments were combined with those following actD alone, TEA + actD, and cycloheximide (CHX) treatments. The rectification index of putative somatic synapses (0-13 µm; n = 10) is higher than the RI of synapses onto proximal dendrites (14-40 µm; n = 50; Kolmogorov-Smirnov Test, *P* < 0.001). Insert: comparison of RI of control samples only; *, *P* <0.05, unpaired t-test. Sites located closer than 14 µm from the tip of the recording electrode were deemed to be putative somatic synapses and were not used for further analysis. **B.** *Top*: Evoked EPSCs were recorded in a stellate cell with a spermine-free pipette solution. The currents were no longer attenuated at +40 mV. *Bottom*: Summary of RI and EPSC amplitude at -60 mV. The EPSC RI is significantly greater than the control recordings (spermine-free: proximal, 8 sites from 6 cells; distal, 7 sites from 4 cells) but is not different between the proximal and the distal sites. ANOVA, P < 0.0001; Tukey post hoc test: ***, *P* < 0.001. **C**. Example cell showing that inclusion of Alexa 488 (20 µM) in the pipette solution reduces apparent rectification of synaptic AMPA receptors. Multiple locations were rapidly screened by placing the stimulation electrode in the vicinity of fluorescent processes (position indicated by circular ROIs).). The processes located in the bottom half of the picture are located deeper into the slice. The corresponding rectification indices for each location are shown in red. Stimulation was performed in the order indicated inside each ROI. Alexa 488 therefore was not used to reveal dendritic morphology in electrophysiology experiments. Right: single focal plane images (top and middle panels) and different focal planes (bottom). **D.** Representative image of a stellate cells filled with Alexa 594 hydrazide via a patch pipette. **E.** Stellate cell dendrites emerge in a star-like, radial manner away from the cell body, as evidenced by the relationship between the geodesic and Cartesian distances measured along each dendrite. *Left*: Cartesian-geodesic distance relationship observed in stellate cells in slices (n=28 dendrites at soma; mean ± SD). Right: Cultured stellate cells also show radial-like spread of their dendrites, albeit with a somewhat higher convolution of their processes.
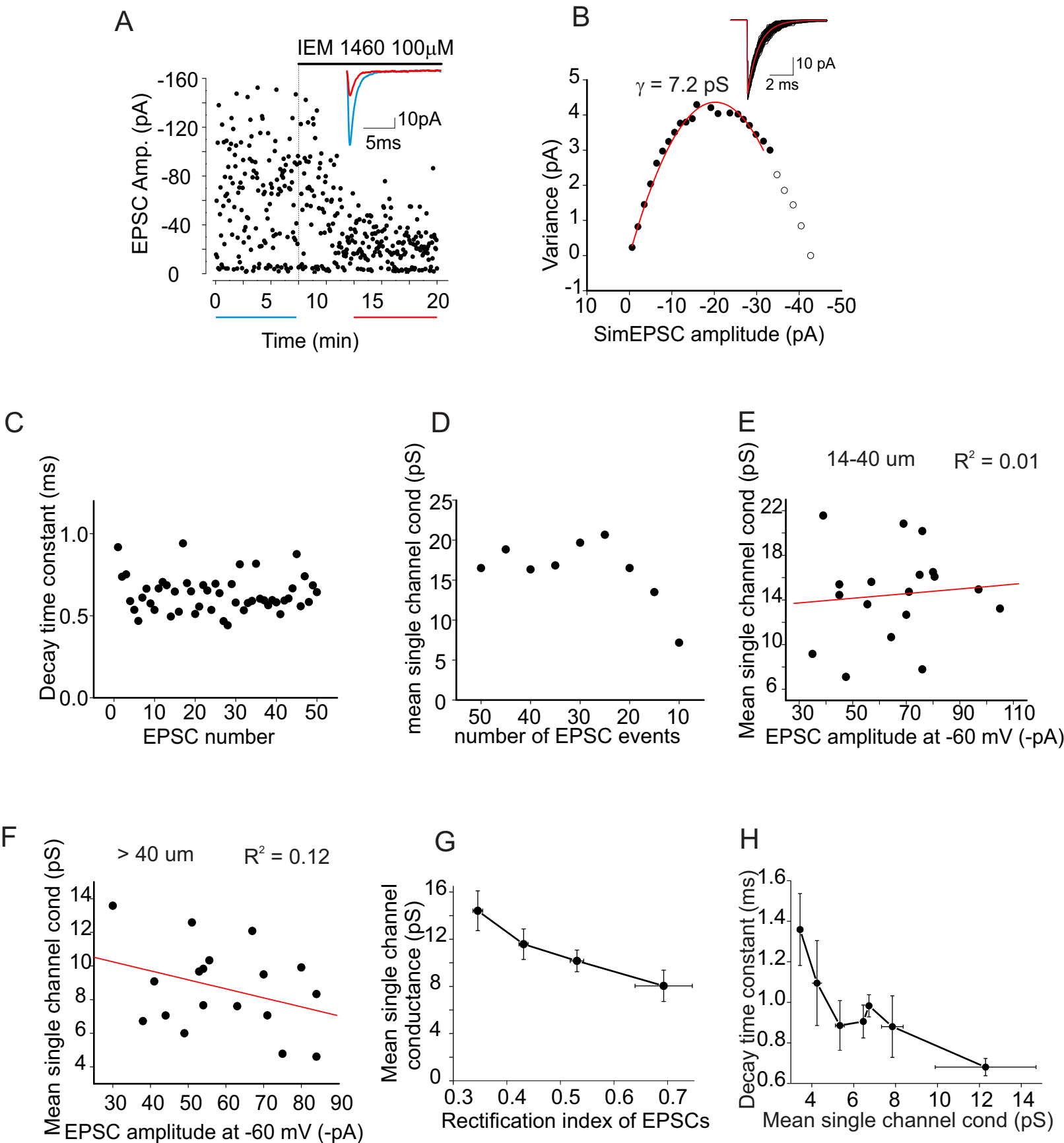
Supplemental Figure 2. IEM-1460 inhibition and single channel conductance of EPSCs, Related to Figure 1**. A**. An example of the time course of IEM-1460 (100 µM) inhibition. **B-H.** Nonstationary fluctuation analysis (NSFA). **B.** Two hundred simulated EPSCs (7.5 pS conductance, 100 channels) and average EPSC (red) Right: Corresponding current – variance plot. The parabolic fit of closed circles (red line) estimated a single channel conductance of 7.2 pS and on average 94 channels open at the peak of the EPSC. **C.** Decay time constant for all individual EPSCs at the synapse shown in the top panel of supplemental Figure 2C. **D**. We compared estimates of single channel conductance from a systematic decreasing number of EPSCs at this synapse (50 to 10 EPSCs). Estimated conductance remained largely unaltered using a data set of 15 or more events. Similar results were also obtained in two other cells tested, consistent with a previous report (Benke et al, 1998). **E-F**. No correlation between estimated single channel conductance and mean EPSC amplitude (14-40 µm range: R^2 = 0.01; n =18; >40 µm: R^2 = 0.12; n = 18). **G**. Mean channel conductance as function of rectification index of EPSCs. Inwardly rectifying EPSCs have a greater mean single channel conductance. **H**. EPSCs with a larger single channel conductance have a more rapid decay time.
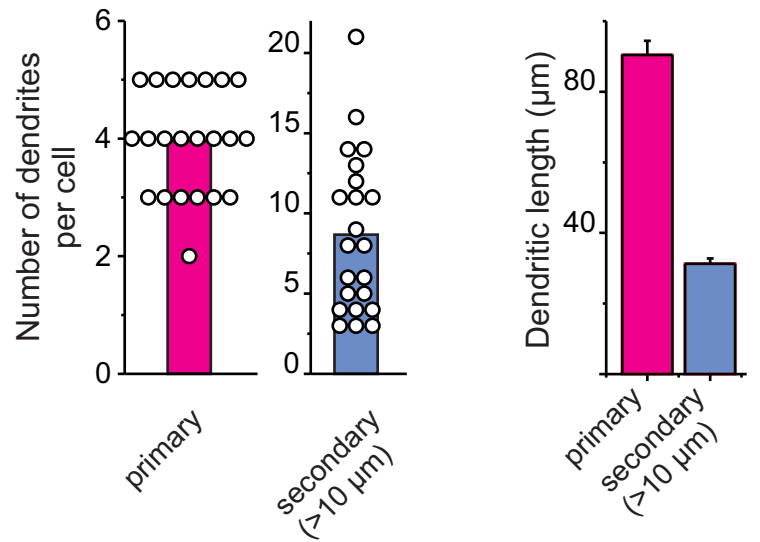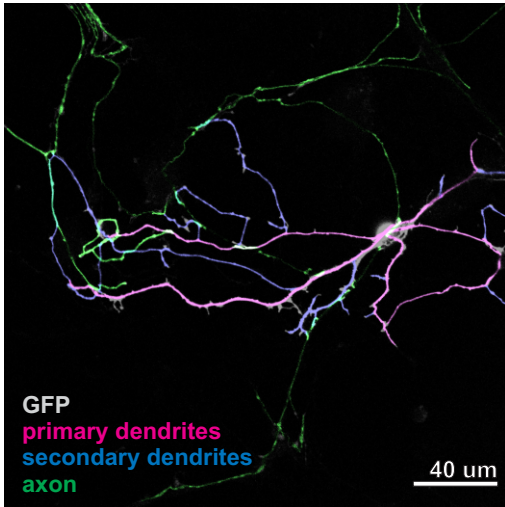
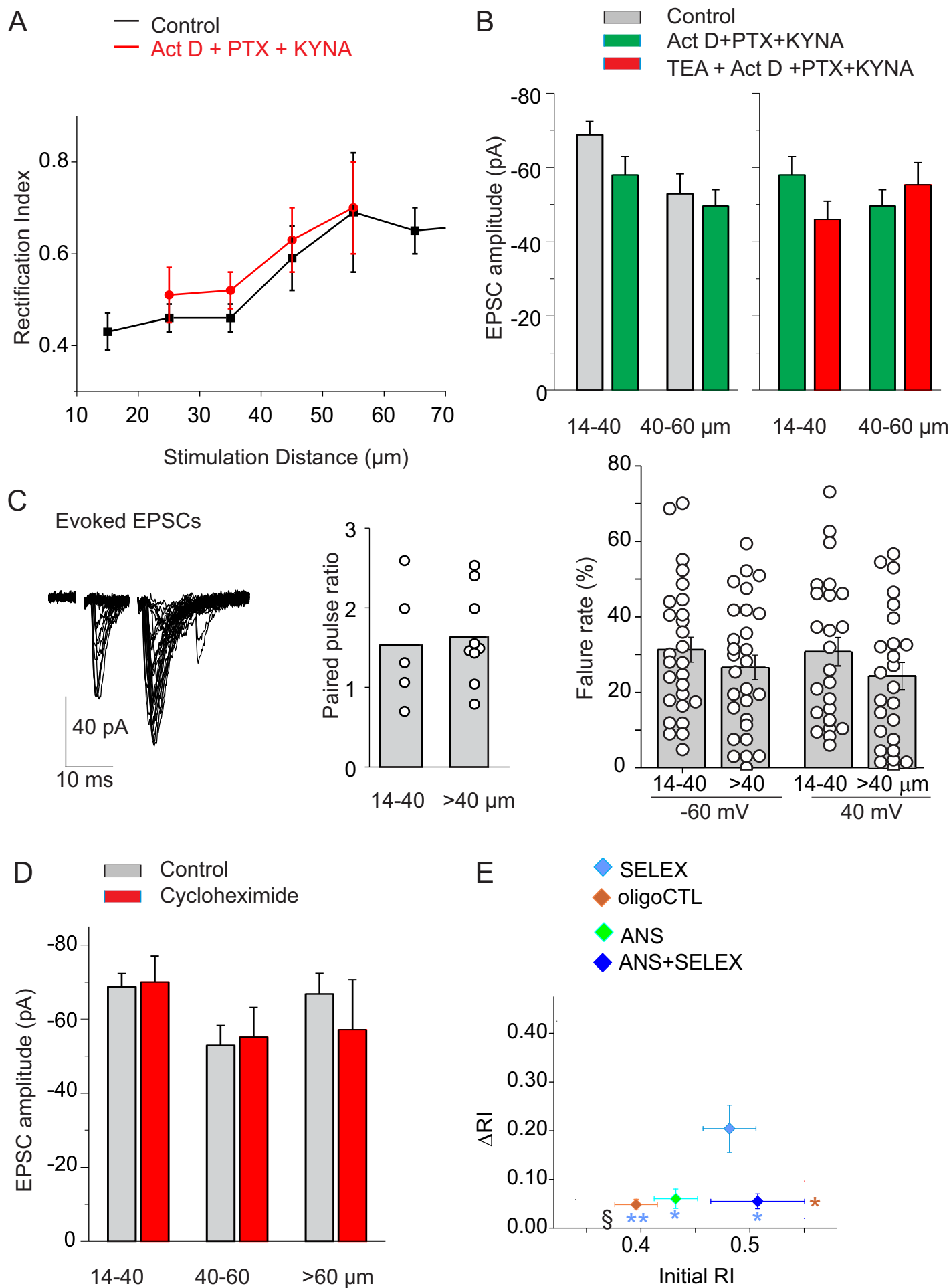**A** Stellate cells in acute slices
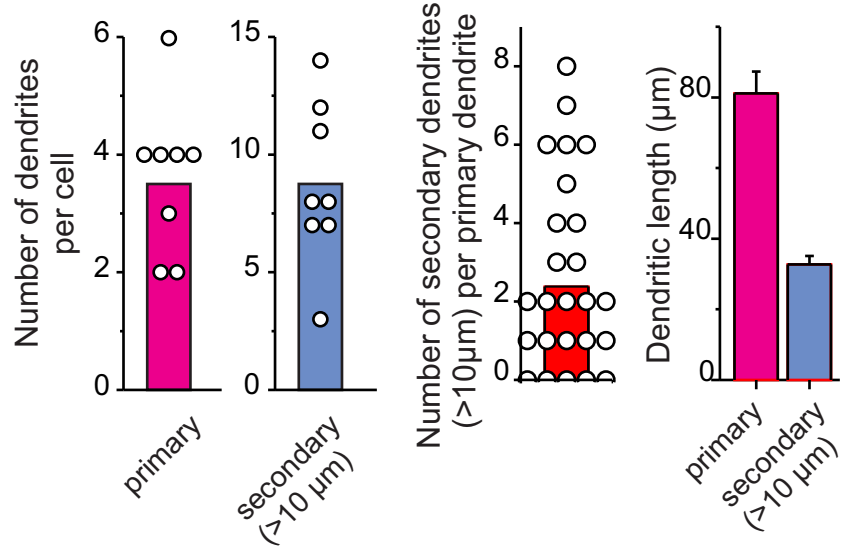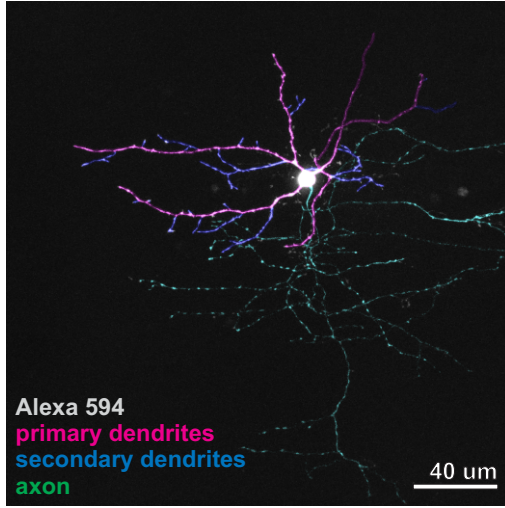
B Stellate cells in primary culture

Supplemental Figure 3, Related to Figure 2. **A**. An example image of a stellate cell in cerebellar slices from P18-23 mice filled with Alex594. Dendrites are shown in red and blue and axons are shown in green. *Bottom*: Summary of dendritic measurements (8 cells). The processes were classified based on their appearance as primary dendrites (thicker processes tapering away from the cell body), secondary processes (emerging from other dendrites), or axon (narrow process of uniform thickness, often with larger varicosities). This image is a maximum projection of a confocal stack taken after fixation but uncorrected for lateral shrinkage. **B**. A representative image of a cultured stellate cell (DIV18-20) from GAD67::GFP mice. Summary of dendritic measurements (22 cells from 3 cultures).

A

Control
Act D + PTX + KYNA

B

Control
Act D+PTX+KYNA
TEA + Act D +PTX+KYNA

C Evoked EPSCs

D

Control
Cycloheximide

E

SELEX
oligoCTL
ANS
ANS+SELEX

Supplemental Figure 4. Related to Figures 3 and 4. **A.** Comparison of rectification index of EPSCs along dendrites between control and ActD (+PTX and KYNA) treatment. The rectification index (RI) increases at distal synapses. The line shows the segmented average (error bars: SEM). **B.** Evoked EPSC amplitude following TEA treatment. Cerebellar slices were incubated with 1 mM TEA and ActD (PTX+KYNA) or ActD (PTX+KYNA) alone as control for 3 hours. **C.** Paired pulse ratio of evoked EPSCs at PF to stellate cell synapses (PPR) was used to estimate glutamate release probability at proximal and distal synapses. Parallel fibers were activated with 2 stimuli separated by 10 ms, while synaptic currents were recorded in stellate cells**.** *Left panel*: example of evoked EPSCs. Average EPSC amplitude of all traces was used to determine the PPR of EPSCs and no difference was found in the PPR between the synapses in proximal and distal dendrites *(middle panel)*. PPR measurement includes both ACSF and Act D incubation (5 proximal sites from 5 cells, average 182.2 sweeps per site; 9 distal sites from 6 cells, average 271.3 sweeps per site). *Right panel*: failure rate of evoked EPSCs did not change with dendritic distance and holding potentials. Open circles are individual data. **D.** Incubation of cerebellar slices with 100 µM cycloheximide for 3 hrs did not alter evoked EPSC amplitude at -60 mV. **E**. Comparison of change in RI (ΔRI) between SELEX and other groups (blue, *), and of initial RI between the CTL oligomer with other groups (brown, *). Only SELEX treatment increases the RI of EPSCs (SELEX, n = 6; CTL oligo, n = 5; ANS, n = 4; ANS + SELEX, n = 4) *, $P < 0.05$.
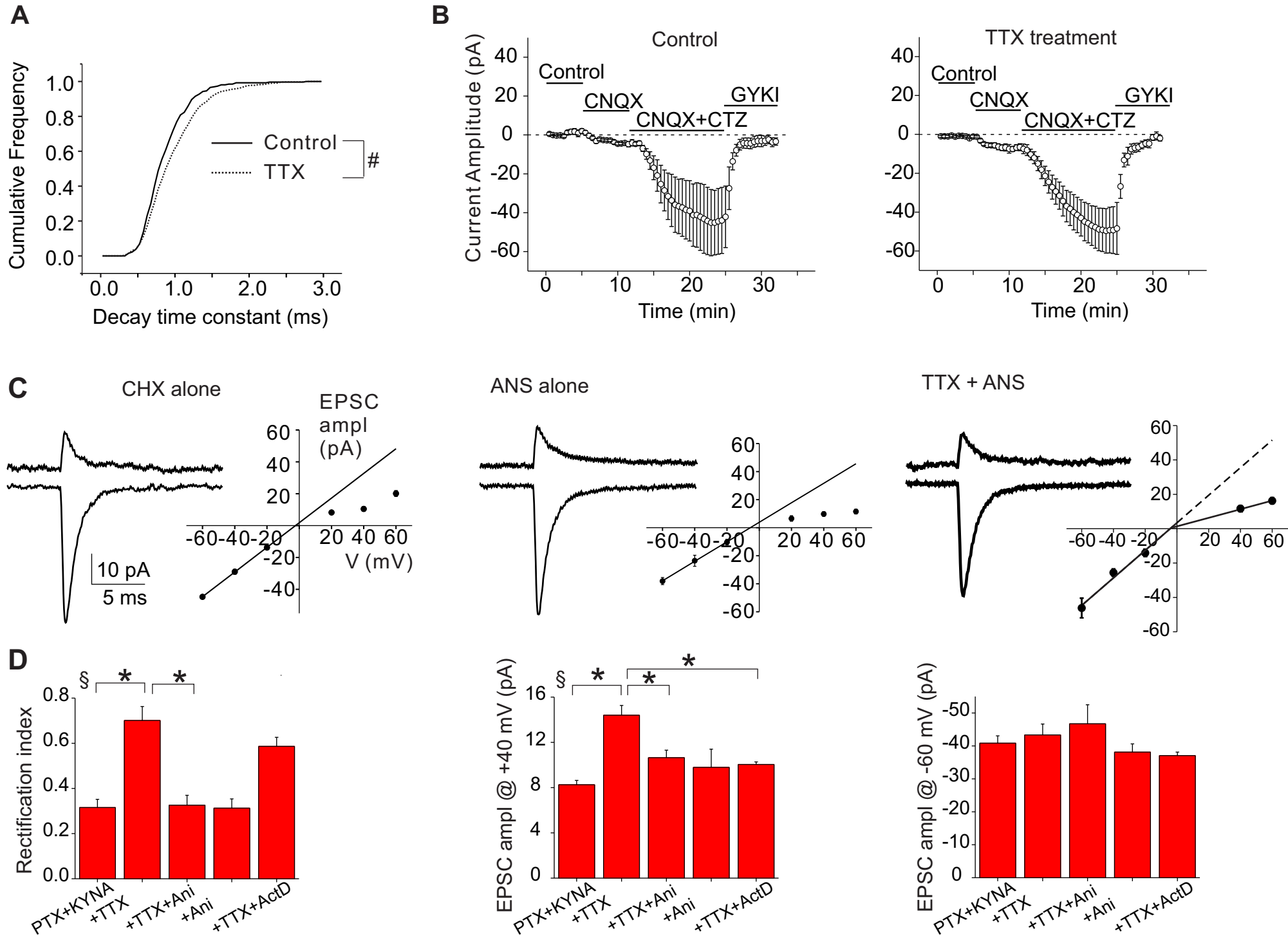
Supplemental Figure 5. Effects of TTX treatment, protein synthesis and transcription inhibitions on AMPARs, Related to Figure 5**. A.** TTX treatment prolongs sEPSC decay time (Kolmogorov-Smirnov Test; P < 0.002; control, 260; TTX, 450 sEPSCs). **B**. TTX-induced switch in synaptic AMPAR subtype does not involve a change in TARP expression. Change in the amplitude of the holding current at -60 mV in response to the application of 10 μM CNQX + 100 μM cyclothiazide (CTZ) (control, n = 4; TTX, n = 5). **C**. Treatment with cycloheximide (CHX) or anisomycin (ANS) alone did not alter the I-V relationship of EPSCs. Anisomycin prevents the TTX-induced increase in rectification of EPSCs. **D**. Summary of rectification index of EPSCs and the amplitude at +40 mV and -60 mV (TTX + Anisomycin, n = 5; TTX + ActD, n = 7). ANOVA test, Tukey test, *, P < 0.05.

A   Spontaneous APs recorded in cultured stellate cells
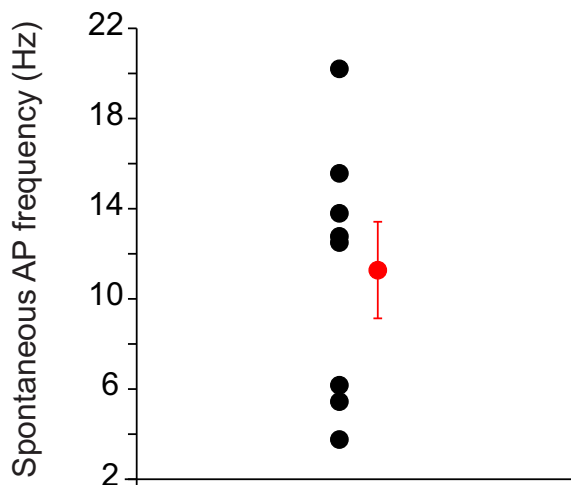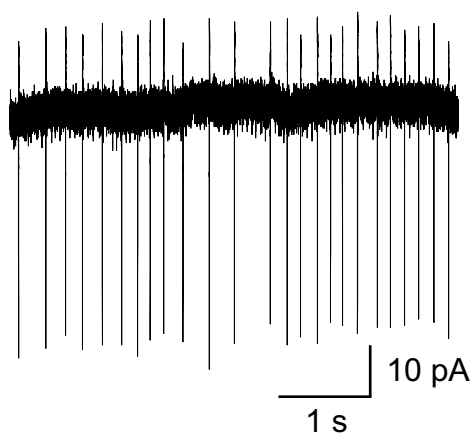
B
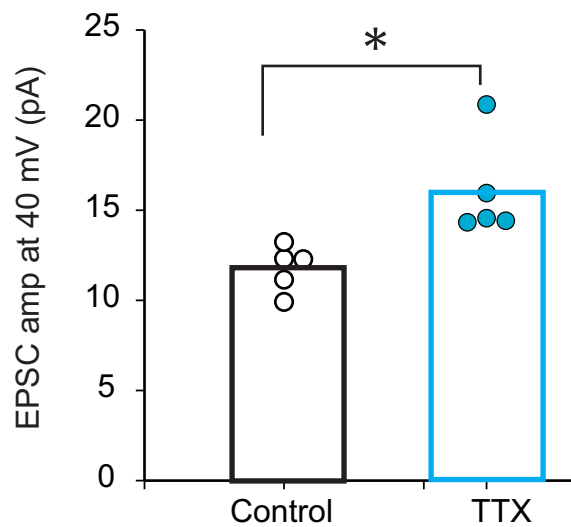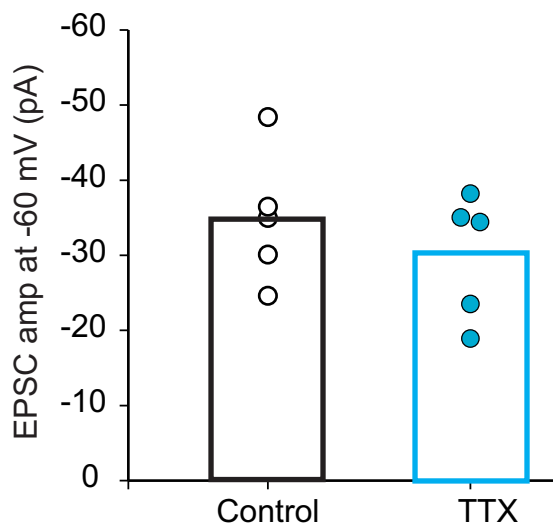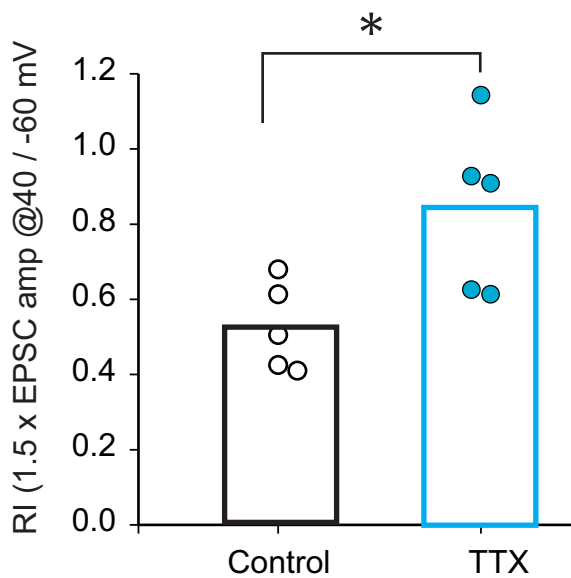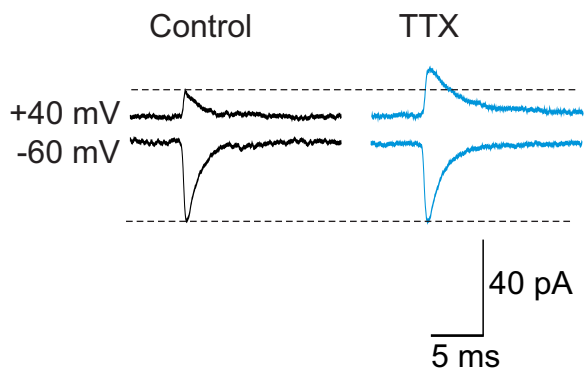
Supplemental Figure 6. Stellate cells in cultures have the same electrophysiological properties as in those in cerebellar slices, Related to Figure 5. **A**. Cultured stellate cells from GAD65::GFP mice are spontaneously active with an AP firing frequency similar to that observed in slice (Liu et al, 2010). **B**. DIV 18 cultures were treated with 0.5 μM TTX (+100 uM PTX + 1 mM KYNA) or with PTX and KYNA (control) for three hours. Spontaneous EPSCs were determined at -60 mV and +40 mV using a pipette solution that contained 100 μM spermine. *Top*, average EPSC amplitude at +40 mV increased after TTX treatment. TTX also increased the rectification index (1.5 x EPSC $_{@40mV}$ / EPSC $_{@-60 mV}$; PTX+KYNA, n=5; TTX, n = 5 from 5 cultures). Thus TTX treatment produce similar effects on synaptic currents and AMPAR subtypes in stellate cells both in culture and slice (Figure 5). *, $P < 0.05$.
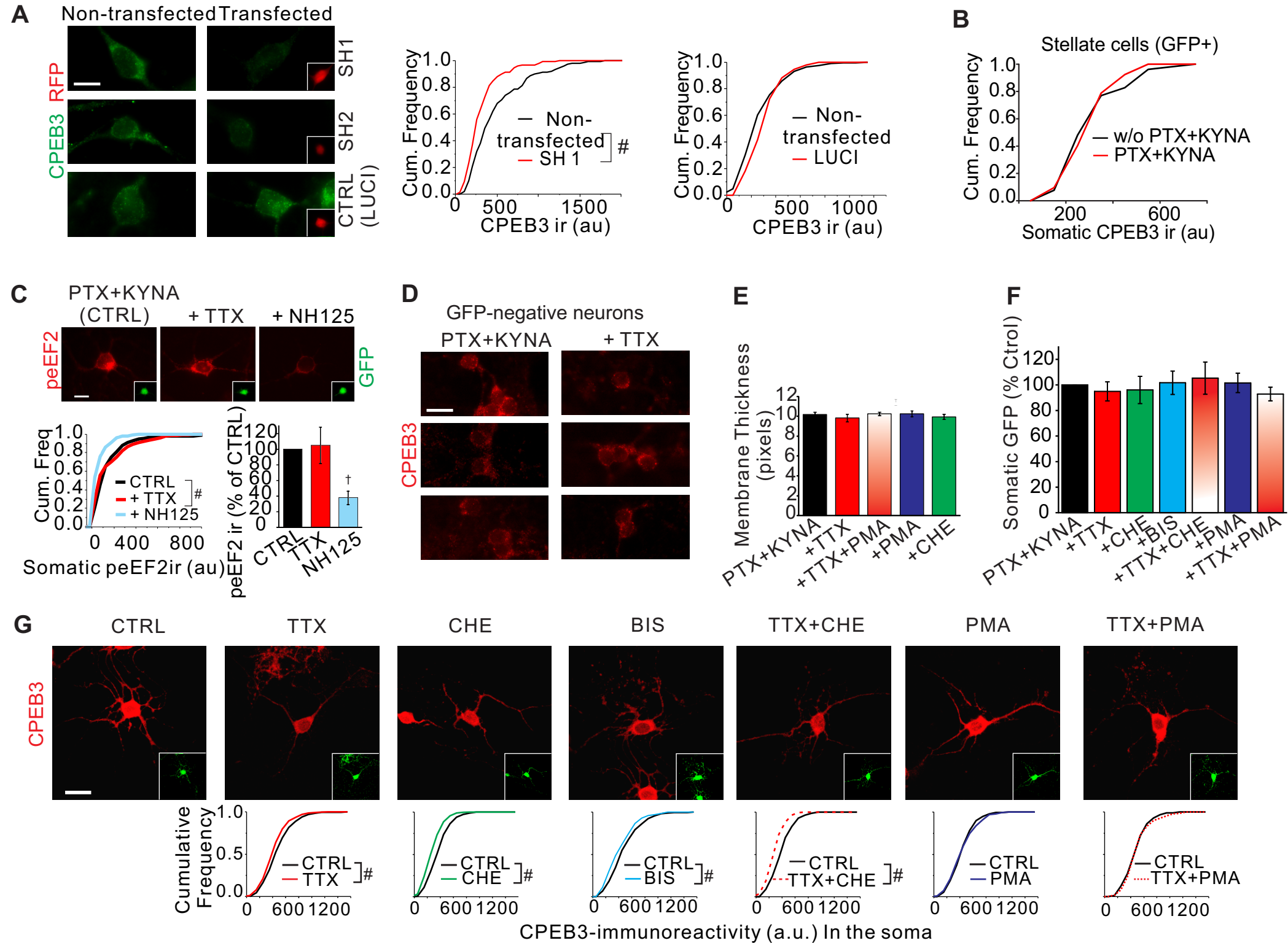
Supplemental Figure 7. Expression and regulation of CPEB3 protein in cerebellar neurons, Related to Figures 5 and 7**. A**. ShRNAs reduce somatic CPEB3 levels in cultured cerebellar cells. *Left*, representative images of CPEB3-ir from cells co-transfected with shRNAs against CPEB3 mRNA (SH1 and SH2) or control shRNA (Luciferase) and a plasmid encoding red fluorescent protein. *Middle*, cumulative distribution of somatic CPEB3-ir in RFP positive cells that express SH1 (90 cells) and in RFP negative cells (197 cells, *P* < 0.0005). *Right*, control shRNA did not reduce somatic CPEB3-ir (94 RFP+ and 131 RFP– cells). **B – D.** Cerebellar cultures were prepared from GAD67-GFP mice and immunostained for CPEB3 or peEF2. **B**. Treatment of cerebellar culture with PTX and KYNA did not alter somatic CPEB3-ir in GFP+ stellate cells. **C**. Phospho-eEF2-ir in the soma of GFP+ neurons was not altered by TTX treatment, but was reduced by treatment with NH125 (10 µM). *Bottom left*, cumulative distributions of somatic p-eEF2-ir (100-222 cells). *Right*, summary graph (one sample t-test, *P* < 0.02). **D**. Examples of somatic CPEB3-ir in GFP– neurons. **E – G**. Effects of PKC inhibitors on somatic CPEB3-ir in stellate cells. **E**. Mean membrane thickness (in pixels, see Methods) from all experiments shown in Fig 7B (21-33 cells). **F.** GFP expression in stellate cells were not affected by treatment with TTX, PKC antagonists and activators. **G**. PKC inhibitors reduced somatic CPEB3-ir levels. Co-application of TTX + PMA restored CPEB3-ir to the control levels (160-222 cells). Scale bars: 20 µm.

A
15 µm
GFP
GluA2
vGlut

B
Rectification index of EPSCs
Total GluA2-ir (size x intensity)
Dendritic distance
10 µm
50 µm
100 µm

C
Size of GluA2-ir
GluA2-ir intensity
clusters / 10 µm
Distance (µm)
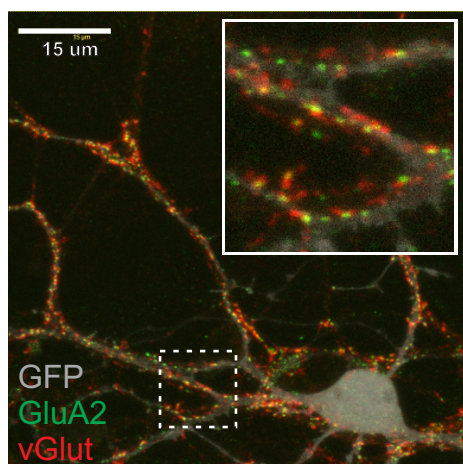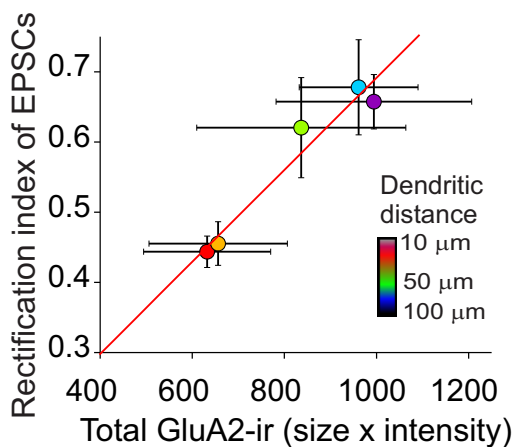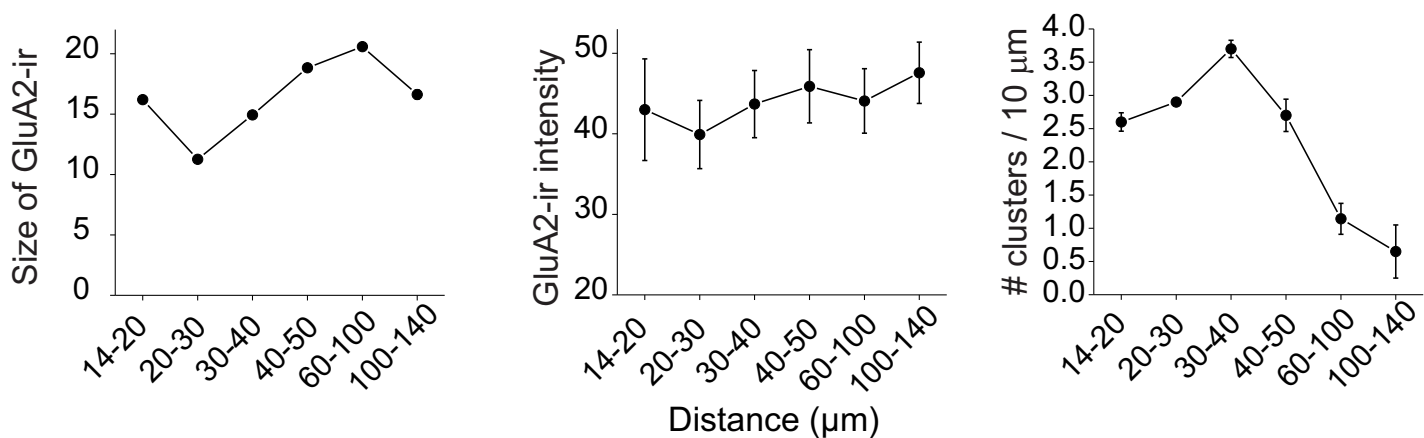
D Mechanisms underlying maintenance of synaptic GluA2 gradient.
Ca²⁺
GluA2 mRNA
Decay   Faster   Slower
Post-synaptic facilitation   Yes   No
GluA2 dendritic gradient   40 µm   60 µm

GluA2-lacking AMPAR
GluA2-containing AMPAR
CPEB3
N-type Ca²⁺channel
Retrograde action potentials

E Functional consequences.
Spontaneous PF activity ("noise")
Burst-like PF activity (sensory input)
~60 µm
~40 µm
EPSP-AP coupling probability
Low
High
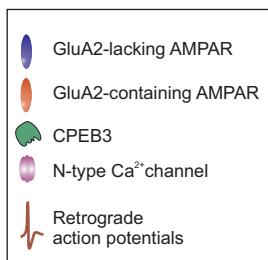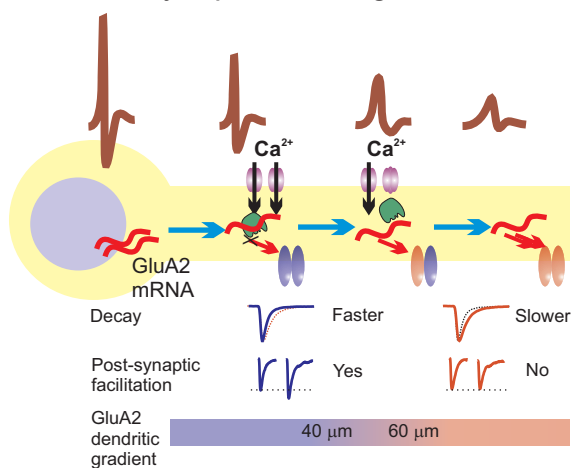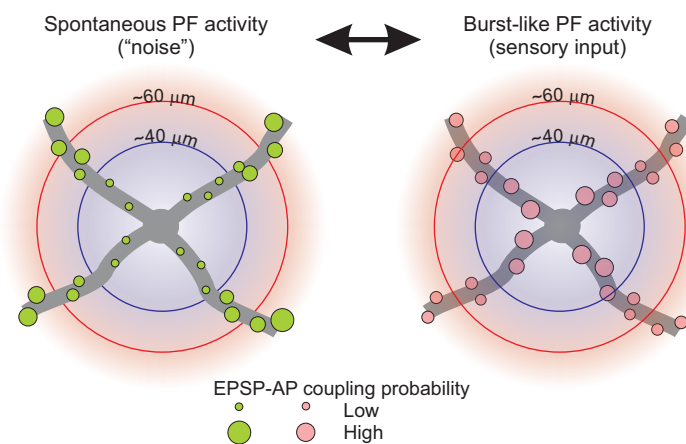
Supplemental Figure 8. A-C. Dendritic GluA2-ir in cultured stellate cells, Related to Figure 6**. A.** Co-immunostaining of GluA2 and vGlut in GAD65::eGFP positive stellate cell in culture shows that GluA2-ir is adjacent to vGlut-ir, suggesting that GluA2-ir are synaptic receptors. **B**. Plot of rectification index of EPSCs in stellate cells in cerebellar slices vs total GluA2-ir (GluA2 cluster size x mean fluorescence intensity) within the same dendritic distance ranges (Red: 14-30, yellow: 30-40, green: 40-50, blue: 50-70, purple: 70-140 μm). Red line, linear correlation (R = 0.98; P < 0.005). **C**. Changes in the size and intensity of GluA2-ir and the number of clusters with dendritic distance. **D and E.** Schematic illustration of a mechanism and possible functional consequences of a GluA2 gradient along dendrites of cerebellar stellate cells. **D.** Somatic APs passively spread backward along dendrites, and both dendritic depolarization and Ca^{2+} entry attenuate with distance (Myoga et al., 2009 and Fig 2). The dendritic depolarization-evoked Ca^{2+} rise activates PKC and thus elevates the CPEB3 levels at proximal dendrites and suppresses GluA2 protein synthesis. Failure to propagate dendritic depolarization to distal sites reduces the CPEB3 level and promotes GluA2 translation. Therefore postsynaptic APs retrogradely control the spatial distribution of synaptic AMPAR subtype by regulating the levels of CPEB3 expression. GluA2-lacking AMPARs at proximal synapses exhibit rapid decay kinetics and a characteristic postsynaptic facilitation due to activity-dependent polyamine unblock by the second stimulus, but GluA2-containing receptors at distal dendrites have a prolonged EPSC decay time and do not display a postsynaptic facilitation (Savtchouk and Liu, 2011). **E**. A GluA2 gradient along dendrites can give rise to a variable postsynaptic response that depends on the location and pattern of presynaptic input. *Left*: We have previously shown that increasing the decay time constant of EPSCs enhances the probability that synaptic inputs evoke APs in stellate cells (Savtchouk and Liu, 2011). Thus GluA2-containing synapses at distal dendrites are predicted to be more likely to trigger an AP in response to a single EPSC, assuming no change in unitary amplitude. *Right*: In contrast, GluA2-lacking AMPARs at proximal synapses would respond more strongly to a train of stimuli because of the polyamine-dependent post-synaptic facilitation observed at these synapses. Therefore distal synapses may specialize in detecting single EPSC inputs whereas proximal inputs might be more effective in triggering an AP doublet in response to paired (burst of) EPSC input such as that observed during sensory activation.

Supplemental Experimental Procedures

Slice preparation and incubation

C57/BL6 mice (postnatal day 18–23) were decapitated in accordance with the animal welfare guidelines of LSU Health Sciences Center and Penn State University. Cerebellar slices were prepared as described previously (Liu et al., 2010; Savtchouk and Liu, 2011). Following decapitation, cerebellar slices (250-300 μm) were obtained with a Leica VT1200 vibrating microslicer. Cerebellar dissection and slicing were performed in an ice-cold slicing solution (mM: 125 NaCl, 2.5 KCl, 0.5 $CaCl_2$, 7 $MgCl_2$, 26 $NaHCO_3$, 1.25 NaH_2PO_4, and 25 glucose, saturated with 95% O_2-5% CO_2, pH 7.4). Slices were maintained in external artificial cerebrospinal fluid (ACSF, in mM: 125 NaCl, 2.5 KCl, 2 $CaCl_2$, 1 $MgCl_2$, 26 $NaHCO_3$, 1.25 NaH_2PO_4, and 25 glucose) at room temperature. In several experiments cerebellar slices were incubated in ACSF containing 1 mM kynurenic acid and 0.1 mM picrotoxin (as control) or with the addition of drugs for at least 3 hours before recording.

Electrophysiology

Whole cell patch clamp recordings were obtained using an Axoclamp 700A or 700B amplifier (Axon Instruments). Stellate cells located in the outer two thirds of the molecular layer were visually identified under DIC using a 60x upright water immersion objective and by the presence of action potentials in the cell attached configuration and spontaneous synaptic currents in the whole cell configuration as described previously (Liu and Cull-Candy, 2000). In cerebellar cultures obtained from GAD65::GFP mice cells that express GFP are stellate cells. Recordings began 10–15 min after obtaining the whole cell configuration. Whole-cell recordings were performed using 5-7 MΩ borosilicate glass pipettes, and the cell series resistance was monitored throughout the experiment. The recording was terminated if the series resistance changed by more than 20-30%. Cerebellar slices were continuously superfused by a gravity-fed system with ACSF containing 0.1 mM picrotoxin. All recordings were performed at room temperature.

Evoked EPSCs. Voltage clamp recordings were performed in sagittal slices using a cesium-based internal solution (in mM: 135 CsCl, 10 EGTA-Cs, 10 HEPES, 4 ATP-Na, 4 MgCl2, 5 TEA, and 1 QX314, pH adjusted to 7.3). To determine the subunit composition of synaptic AMPA receptors, 100 μM spermine was included in the internal solution unless otherwise indicated. Spermine and endogenous polyamines block GluA2-lacking (but not GluA2-containing) AMPARs at positive potentials. Therefore, synaptic GluA2 content at a synapse was assessed by comparing the synaptic conductance at positive and negative potentials from the I-V relationship. Synaptic AMPAR currents were evoked by placing a monopolar glass stimulating electrode filled with ACSF at various distances from the soma of a patched cell and applying brief (~400 μs) voltage pulses (5-25 V) in the presence of 200 μM PTX and 10 μM R-CPP at 0.3 Hz to block GABA and NMDA receptors, respectively. The stimulation strength was adjusted such that 50% of stimuli evoked EPSCs to minimize stimulation of multiple synapses. Evoked EPSCs are often unitary events, but we cannot rule out that we might stimulate two (or more) neighboring synapses at some locations.

Stellate cells send their dendrites radially within the sagittal plane of the cerebellar folium and parallel fibers (granule cell axons) extend orthogonally to the stellate cell dendrites. Therefore the sagittal slice preparation provides a restricted stimulation of synapses (Soler-Llavina and Sabatini, 2006, Abrahamsson et al. 2012). To achieve a local, targeted activation of the parallel fibers we used a stimulation pipette with a small opening (5-8 MΩ), ejecting minimal currents to achieve threshold stimulation (50% failure rate). Such stimulation was spatially specific because purposefully moving the electrode by several μm sideways often drastically increased the failure rate ("lost" input), consistent with previous studies using either Ca^{2+} imaging in stellate cell dendrites (Soler-Llavina and Sabatini, 2006) or optical detection of extracellular glutamate released upon parallel fiber stimulation (Okubo et al. 2010).

As expected we observed a close correlation between the dendritic length and stimulation distance within the sagittal plane, with stimulation sites more distant from the stellate cell body corresponding to the more distal synapses, as shown in Suppl. Fig 1E. To obtain the current-voltage relationship, synaptic currents were recorded at various potentials (between -60 and +40 mV) by pseudo-randomly voltage-clamping a postsynaptic cell at a given holding potential while evoking a synaptic current. Between 70 and 200 sweeps were collected at each potential at every stimulation site. IEM-1460, a GluA2-lacking AMPAR blocker, was also used to identify AMPAR subtype. We recorded evoked EPSCs at the same synapses in a stellate cell before and during a bath application of IEM-1460 (100 μM). Because IEM-1460 is an open channel blocker, we stimulated parallel fibers during IEM-1460 application. The recordings were low-pass filtered at 6 kHz and digitized at 20 kHz using a Digidata 1320. For rectification index of EPSCs along dendrites we recorded EPSCs at 1-4 synaptic sites/cell. Because it is difficult to completely washout IEM-1460 its effects was only determined at 1 synaptic site from each cell. On average 1-2 cell from each animal.

Analysis: The EPSC amplitude was plotted at each potential to produce an *I–V* relationship. The mean EPSC amplitudes at negative potentials were fitted by linear regression. The rectification index (RI) of the *I–V* relationship was defined as the ratio of the current amplitude at +40 mV to the predicted linear value at +40 mV (extrapolated from linear fitting of the currents at negative potentials) as described previously (Liu et al, 2010). The current amplitude at each potential was measured using several methods: 1) peak of the average of all sweeps at each potential, 2) average of the current peaks (within a 2-3 ms window after the stimulation artifact) of all sweeps at that potential, 3) same as 2, but with failure removal. All three methods produced very similar results, but we ultimately used method 2 for calculating the rectification index because this minimized the error caused by the synaptic jitter, and produced the best linear fit at negative potentials. Method number 3 was not used for RI because of the possibility of removal of smaller events. In addition to RI, we also calculated Rectification Ratio (I @ +40 / I @ -40 mV), and voltage-normalized Rectification Ratio (I @ +40 / I @ -60 mV x 1.5); in most cases all three produced very similar results. Only the stellate cells with at least 2 measured stimulation sites were included in our analysis. In order to obtain the most accurate amplitude and decay measurements of individual synaptic currents at -60 mV, we manually selected individual events exhibiting a smooth rise and decay phase to avoid including multiple release cases. Additionally our use of threshold stimulation helped to minimize the recruitment of multiple synapses. The manually selected EPSCs were

aligned and the resulting average waveform was fitted with a single component exponential decay function. Multiple exponential fit generally produced similar results as previously reported (Savtchouk and Liu, 2011). For IEM-1460 experiments, we found that maximal inhibition occurred at about 7.5 min, and therefore the measurement of EPSCs were taken 7.5 min following IEM-1460 exposure. Only cells with stable recordings prior to IEM-1460 application were analyzed and failure rate did not change throughout the recordings. Failures were removed to calculate average EPSCs and % inhibition of IEM-1460.

Non-stationary fluctuation analysis (NSFA) was performed as described previously (Benke et al., 1998; Tranelis et al, 1993). EPSCs were selected from events used for measurements of decay time of individual synaptic currents at -60 mV. These EPSCs have a fast rise time and stable baseline holding current, and are not contaminated by multiple release and spontaneous synaptic currents. EPSCs were aligned at the fast point of the rise time and the average EPSC was scaled to the peak of individual simulated or evoked synaptic currents. The decay phase of an EPSC was divided into 30 equal sections from the EPSC peak to 5-6 times the decay time. The variance of the EPSC decay phase about the mean was then calculated for each section and plotted as a function of the mean current amplitude. The mean single channel current (i) was estimated by fitting the initial 50%, 75% and 100% of maximal amplitude to Variance = i(current) − (current)^2/N + baseline variance, where N is the number of channels activated at the peak of EPSCs. If the variance-current relationship was skewed towards larger currents, only the initial 50% and 75% of the data were used to estimate the conductance. The estimated conductances from different portions of the same variance-current plot were similar. Simulated EPSCs were constructed from single channel openings as described previously (Traynelis et al. 1993) and were used to test the feasibility of the method. When simEPSCs of 5, 7.5, 10 and 20 pS conductance (50, 100, 200 channels; 1 ms and 2 ms decay time constant; 100 and 200 simEPSCs) were tested, the correct conductance was obtained (Suppl. Fig 2A). However inclusion of a few events with the same conductance but different decay kinetics (thus channel opening time), markedly increased the calculated channel conductance. By using threshold PF stimulation in sagittal slices we reduced the chances of activating multiple synapses. However upon analysis of decay time constants of evoked EPSCs, a small fraction of events at some synapses displayed markedly different kinetics and gave rise to a greater (EPSC(t) − scaled avEPSC(t))^2 than simulated EPSCs at all conductances. These synaptic events are likely to originate from different synapses and were therefore not included in the data set. We systematically reduced the number of EPSCs used for analysis and determined that a minimum of 15 events was required to obtain an accurate estimate of conductance (Suppl. Fig2B), consistent with previous observations by Benke et al (1998).

Dendritic distance measurements: In a few pilot experiments we included 20 µM Alexa Fluor 488 in the pipette solution to visualize the dendritic processes and more accurately measure the synaptic distance. However Alexa 488, when included in the pipette solution, alters the rectification index of EPSCs (suppl. Fig 1C), and therefore was not used to reveal dendritic morphology in electrophysiology experiments. In cells filled with Alexa 594 a direct comparison between the Cartesian distance with geodesic dendritic distance showed a close correlation (R^2 = 0.999) and Cartesian distance underestimated dendritic length by ~15% at 40-110 µm (Suppl. Fig 1E). We therefore estimated the dendritic length by the Cartesian

distance between recording and stimulating electrodes. Images of the recording and stimulating electrode locations were captured at different focal planes and stored for off-line analysis. Since the parallel fibers run orthogonally to the dendritic plane of the stellate cell, we calculated the synaptic distance as a Cartesian distance (i.e. straight line) between the z-projections of the patch electrode and each stimulation electrode onto the same plane. Thus Cartesian distance is referred to as "dendritic distance". The synaptic currents evoked at sites located less than 13 µm from the recording electrode could be mediated by somatic synapses and were therefore excluded (suppl. Fig 2A).

CPEB3 oligonucleotide (Aptamer) experiments: To examine whether CPEB3 was involved in the synaptic GluA2 gradient, we used a synthetic RNA oligonucleotide sequence previously shown to disrupt the interaction of GluA2 mRNA and CPEB3 (Huang et al, 2006). We patched each stellate cell with an intracellular solution containing 10 µM SELEX1904 aptamer (synthesized by IDT) while testing for changes in eEPSC rectification with time to determine GluA2 incorporation over a period of 1-2 hours. In order to reduce the total number of stimulations and to improve our temporal resolution to detect a fast change in the RI of the synapse, we used a reduced IV protocol, by recording the evoked currents at +40, 0, -40, and -60 mV. Additionally, the number of stimulations at 0 mV was reduced by half. To verify that the effect of this SELEX1904 aptamer was shown to be sequence- and structure-specific, we also utilized a control aptamer containing a shorter sequence (SELEX1904-short, a 25 bp sequence that comprises the binding sequence but not the hairpin loop tail of the full 49 bp sequence) that does not maintain the hairpin structure required for CPEB3 binding. SELEX1904 sequence: GGGAGAAUUCCGACCAGAAGAAAGAGGAUUUGUGUUUUUCAGGACUAUGUGCGUCUACAUGGAUCCUCA. Control (a short oligo): AAAGAGGAUUUGUGUUUUUCAGGAC.

Spontaneous EPSCs and CNQX-evoked currents: Spontaneous EPSCs were recorded at various holding potentials (from –60 to +60 mV) and were filtered at 2 kHz and digitized at 20 kHz. The average current trace at each holding potential (typically 20–40 sEPSCs) was constructed by aligning each event on its point of fastest rise using N version 4.0 (Dr. Steve Traynelis, Emory University). Events that did not have a smooth rise and decay phase were rejected. CNQX (10 µM) and cyclothiazide (100 µM)-induced currents were recorded in ACSF containing 100 µM picrotoxin, 20 µM D-AP5, 3 µM strychnine and 0.5 µM TTX to block $GABA_A$, NMDA and glycine receptors, and Na^+ channels, respectively. GYKI52466 (50 µM), an AMPAR blocker, was applied at the end of each recording to confirm that the current was mediated by AMPA receptors.

Ca imaging. For Ca^{2+} imaging experiments (Gasparini, 2011), whole-cell patch-clamp somatic recordings were performed using a Dagan BVC-700 amplifier in the active 'bridge' mode. Trains of 5 somatic action potentials at 100 Hz were elicited by the injection of brief current steps (300-600 pA, 2 ms-duration each). Patch pipettes were filled with a solution containing (in mM): K-methylsulphonate 130, HEPES 10, NaCl 4, Mg_2ATP 4, $Tris_2GTP$ 0.3, phosphocreatine 14, and Oregon Green BAPTA-1 (OGB-1) hexapotassium salt 0.1; the resistance of the electrodes was 4-6 MΩ. OGB-1 was excited using a Chameleon Ultra laser (Coherent, Santa Clara, CA) emitting ultra-fast, pulsed light at 920 nm; the emitted fluorescence was detected using an Ultima scanner (Prairie Technologies, Madison, WI) mounted over an Olympus (Center Valley, PA) BX61WI microscope. Dendritic changes in $[Ca^{2+}]_i$ associated with the train of somatic spikes were quantified by calculating $\Delta F/F$, where F is the resting

21

fluorescence intensity, after subtracting autofluorescence, and ΔF is the change in fluorescence caused by dendritic depolarization (Lasser-Ross et al., 1991). The autofluorescence of the tissue was measured by line scans of regions of comparable size near the dye-filled dendrite. Line scans were repeated five to ten times at a single location and averaged. The dendritic length was determined as the distance from the center of the stellate cell by tracing the individual dendrites to the location where the Ca^{2+} transients were measured.

Dendritic structure of stellate cells. To visualize dendrites of stellate cells, we included 0.5 mM Alexa 594 hydrazide in the electrode and patched stellate cells in sagittal cerebellar slices as described previously (Rieubland et al, 2014). The electrode was slowly removed 15 min after obtaining the whole cell configuration and cerebellar slices were fixed in 4% paraformaldehyde in PBS for 2 hrs. Confocal images of dendritic Alexa 594 fluorescence were acquired with a TCS SP2 SE Leica confocal microscope (63x objective) and analyzed using ImageJ 1.46r software (NIH). Dendrites were traced using ImageJ plugin NeuronJ (Meijering *et al*. 2004) and analyzed using a custom macro script. For these purposes, the primary dendrites are defined as the longest processes emanating directly from the soma, and secondary dendrites are all branches longer than 10 µm as defined previously (Myoga et al. 2009). Dendritic length was corrected for the shrinkage in the sagittal plane due to fixation by multiplying by 1.09, as determined previously (Rieubland et al, 2014).

Primary cerebellar cell culture

Cerebellar cell cultures were prepared using P7 wildtype and mutant mouse pups expressing eGFP under the GAD65 (GAD65::GFP) or GAD67 promoter (GAD67::GFP; from the Jackson Lab). The culture protocol was as previously described (Fiszman et al 2005) with several modifications. Briefly, the cerebellum was chopped and trypsinized (6 mg typsin / 5 ml) for 50 minutes at 37°C. Following digestion, the tissue was triturated, centrifuged, and resuspended in basal medium eagle (supplemented with 10% FCS, 0.1 mg/ml h-transferrin, 7 mM KCl). The resulting cell suspension was plated onto poly-D-lysine coated coverslips for one day, at which point half of the medium was replaced with Neurobasal medium supplemented with B27. At DIV4, 10 µM cytosine arabinoside was added directly to each dish to inhibit glial proliferation. Cells were maintained for 18-27 days *in vitro* at 37°C in 5% CO_2. Stellate cells were visually identified by green fluorescent protein expression.

Pharmacological treatment of cerebellar cultures.

One mM kynurenic acid (Ascent) and 0.1 mM picrotoxin were added to all incubation solutions, including controls. Cerebellar cultures from GAD65::GFP mice were used for experiments described in Fig 5 and 6. The following drugs were included in the culture medium: 0.5 µM TTX (Ascent)**,** 1 µM chelerythrine chloride, 300 nM bisindolylmaleimide (Calbiochem), 100 nM phorbol 12-myristate 13-acetate, 10 µM NH125. The cultures were then returned to the incubator for 3 hrs. Both experimental and control dishes contained the vehicle as needed (0.1% DMSO). Other drugs were obtained from Tocris. For dendritic CPEB3 staining experiments, cultures made from GAD-67 mice were incubated for 3 hours in HEPES-based extracellular solution (in mM: 135 NaCl, 3 KCl, 2 $CaCl_2$, 1 $MgCl_2$, 10 HEPES, 11

glucose; pH adjusted to 7.3 with 1M NaOH) at room temperature with TEA and ω-conotoxin GVIA to match our slice treatment conditions. The treatment groups were as follows: control (200 μM picrotoxin, 2 mM kynurenic acid), ω-CTX (0.5 μM), TEA+ActD (1 mM TEA, 25 μM Actinomycin D), and ActD alone (25 μM) in addition to PTX and KA. Each experiment was repeated at least 3 times using different cultures, and all treatment conditions were performed on each batch of dishes. The presence of KYNA and PTX (control) did not alter CPEB3-ir in stellate cells (suppl. Fig 7B).

Immunocytochemistry

To test the selectivity of a CPEB3 antibody, we transfected cultures with two shRNAs for CPEB3, which have previously shown to increase the expression of GluA2 protein (Huang et al., 2006; Pavlopoulos et al., 2012; Wang and Cooper, 2009). Two previously described shRNA sequences designed against CPEB3 mRNA, Sh1 (top strand: CCGTACGTGCTGGATGAT) and Sh2 (CGTACGTGCTGGATGATA) (Huang et al., 2006; Wang and Cooper, 2009) were subcloned into pSIREN-RetroQ-DsRed-Express (Clontech). Transfection of cultured neurons from wild-type mice was performed on DIV5 using a calcium-phosphate protocol and the cultures were stained for CPEB3 on DIV9. We observed a reduction of CPEB3-ir of 38 ± 2 % with shRNA#1 and 28 ± 14 % with shRNA#2 compared to non-transfected cells, whereas expression of a control shRNA (luciferase), which did not target CPEB3 failed to reduce the level of CPEB3-ir (Suppl. Fig 7A).

Cultured cerebellar neurons were washed in PBS and fixed in 4% paraformaldehyde in PBS for 20 minutes. When staining with the PKC antibody, the cultures were fixed without washing. Following a 15 minute permeabilization with PBS containing 0.3% Triton, the cultures were blocked with 3-5% BSA (or 5 % goat serum with 0.05% Triton-X in PBS) for 30 minutes. Cultures were incubated with primary antibody in blocking solution for 1 hour at room temperature. After 4 washes in PBS the secondary antibody was applied for 1 hour, followed by PBS wash (4 times) before the coverslip was mounted. After PKC staining, RedDot, a nuclear marker, (1:50) was added for 30 minutes after the last wash. We used the following antibodies: rabbit CPEB3 (1:100, ABCAM), rabbit Phospho-eEF2 (1:100, Cell Signaling), guinea pig Vglut (1:1000, Chemicon); rabbit MAP2 (1:500, Millipore), mouse PKC-αβγ- (1:100, Millipore), donkey anti-mouse DyLight549 (1:100, Jackson), donkey anti-rabbit DyLight549 (1:100, Jackson), donkey anti-rabbit Alexa488 (1:200, Invitrogen) and donkey anti-rabbit CF-633 (1:250, Biotium). In two sets of experiments (Suppl Fig 7G; and Fig 5C) cultures were incubated in rabbit CPEB3 antibody (1:200 and 1:100, respectively) for 12 hours at 4°C. No immunostaining was evident when the primary antibody was omitted.

Immunostaining for surface GluA2 proteins under non-permeabilizing conditions (without Triton-X): cerebellar cultures were fixed in 4% paraformaldehyde for 8 minutes. The cultures were blocked with 3-5% BSA (or 5 % goat serum in PBS) for 30 minutes, and was double stained with mouse anti-GluA2 raised against an external epitope (1:200; Cell Signaling) and rabbit anti-MAP-2 antibody (1:500; Millipore) then secondary donkey anti mouse Cy3 (1:400) and anti-rabbit CF-633 (1:1000).

Image analysis

Confocal images of dendritic GluA2, MAP2 and GFP fluorescence (or CPEB3, p-eEF2) were acquired with a TCS SP2 SE Leica confocal microscope (63x objective with 2x or 4x zoom, 0.2 µm step) and analyzed using ImageJ in a blind manner. Because granule cells also express GluA2, CPEB3 and p-eEF2, we avoided areas with high cell density or where dendrites were adjacent to non-fluorescent processes (i.e. "bundles" of axons or dendrites). Although intensity of GFP signals varies from cell to cell, average GFP signals of stellate cells used for analysis were not different between experimental conditions (Fig 6C and Suppl Fig 7F). Furthermore, the GFP signal was applied as a mask to both channels in order to exclude any fluorescent signal outside the process. GluA2-ir images were linearized using the Straighten plugin for ImageJ (Kocsis *et al*. 1991) as previously described (Sutton *et al*. 2007). The threshold for detecting GluA2-ir clusters was set to the average red fluorescence + 2 SD in each GFP positive process and the total fluorescence of each cluster along the GFP processes was determined using the "Analyze Particles" function and a custom macro in ImageJ. In order to restrict our analysis to surface GluA2 only, we performed staining in the absence of detergent (Trigon X-100) and in the presence of an antibody against an intracellular dendritic marker, MAP2. Consequently, any process that showed positive MAP2 staining was considered as spontaneously permeabilized and was discarded.

For the analysis of dendritic CPEB3-ir and p-eEF2-ir multiple ROIs (regions of interest, circles of the same size) were placed starting at the center of the soma and along a dendrite of the fluorescent cell, and the average fluorescence in each channel was calculated for each ROI, discarding any ROIs with any pixel saturation present in either of the channels. Raw fluorescence in both channels (red and green) was masked using GFP channel, keeping only the pixels whose GFP (green) value was above a fixed threshold, and the intensity of the remaining pixels was then averaged in each ROI. A decrease in the average GFP fluorescence in Fig 6C (right) reflects a reduction in the diameter of dendritic processes because the average GFP fluorescence was calculated for each ROI along dendrites. To account for changes in dendritic diameter a CPEB3/GFP (red/green) ratio was calculated for each ROI. Additionally, because GFP levels in GABAergic interneurons vary from cell to cell, the ratio of CPEB3-ir/GFP along a process was normalized to the ratio at 5-14 µm. This would allow us to determine changes in the CPEB3-ir along each process (independently of changes in process thickness or morphology), and to compare them between different experimental conditions. For presentation purposes in Fig 6A, the ratio of CPEB3/GFP along dendrites was smoothened with a three-point running average and displayed as a pseudocolored overlay inside each individual ROI using "Rainbow RGB" color lookup table (ImageJ), after which the images were converted to RGB colorspace and straightened. For GluA2-ir, the puncta were detected using ImageJ "analyze particles" command on the GluA2 channel by setting the threshold to 2 standard deviation above the mean GluA2 level within the dendrite. Total fluorescence for each punctum was calculated as the average GluA2 signal within each punctum times the area, corresponding to the total number of GluA2 molecules present at the synapse. In Figure 6E we have re-colored each GluA2 puncta according to their total fluorescence, using a nonlinear ("Jet") color scale. This is because the human visual system is believed to largely under-estimate any small linear changes in either brightness or area of a visual object, with *perceived* changes roughly proportional to the root or the logarithm of the *actual* change in magnitude (Weber–Fechner law, Stevens' power law).

For analysis of CPEB3 immunoreactivity in the soma of cerebellar neurons, images were acquired at 60x with an Eclipse TE2000-U fluorescent microscope (Nikon). Only isolated neurons were selected for analysis and the fluorescence intensity was quantified using ImageJ. Two dishes from the same culture were subject to each treatment and a minimum of 30 cells in each condition were analyzed. Each experiment was repeated at least 3 times.

To analyze PKC translocation, confocal images of isolated cells were acquired. From line plot profiles (intensity of each point along the line) of PKC-ir across the plasma membrane of the PMA treated cells, we established that the width of the PKC membrane signal was 8.5 ± 0.8 pixels, (n = 6 cells, 4 lines per cell), as estimated from the width at the half point of the signal peak (Fig 7A). Selection of the different compartments (membrane, cytoplasm and nucleus) was performed based on GFP signals, PKC-ir and nuclear staining as shown in Fig 7A. To characterize the compartmental distribution of PKC-ir in each cell, the integrated density (sum of all pixels values) of each compartment was divided by the whole cell integrated density and the percentage calculated. As an alternative approach to quantify the translocation of PKC we calculated the ratio between membrane and cytoplasm mean intensity (integrated density/number of pixels). To determine whether the selection of the membrane was similar in all conditions, we also calculated the membrane thickness using $A/((P1+P2)/2)$, where A is the area of cell periphery that was selected as delimiting the cell membrane, P1 is the external perimeter of the membrane and P2 the internal perimeter of the membrane staining (Suppl. Fig 7E). Eight cells were analyzed per experimental condition and the experiment was replicated 4 times.

Statistics: All values are expressed as mean ± S.E.M. Statistical significance was assessed using ANOVA, repeated measures ANOVA, or Student's *t* tests (paired, unpaired two-tailed or one sample) as appropriate if a data set passed the Shapiro-Wilk normality test. Otherwise, Mann-Whitney test and Wilcoxon signed rank test were used. The Kolmogorov–Smirnov test was used for comparison of cumulative distribution plots. Summary of statistical analysis are shown in suppl. Table 1.

Supplementary references

Abrahamsson, T., Cathala, L., Matsui, K., Shigemoto, R., and Digregorio, D. A. (2010). Thin dendrites of cerebellar interneurons confer sublinear synaptic integration and a gradient of short-term plasticity. Neuron *73*, 1159-1172.

Benke TA, Lüthi A, Isaac JT, Collingridge GL. (1998) Modulation of AMPA receptor unitary conductance by synaptic activity. Nature. 393:793-7.

Gasparini S. (2011) Distance- and activity-dependent modulation of spike back-propagation in layer V pyramidal neurons of the medial entorhinal cortex. J. Neurophysiol.105:1372-9.

Huang, Y. S., Kan, M. C., Lin, C. L., and Richter, J. D. (2006). CPEB3 and CPEB4 in neurons: analysis of RNA-binding specificity and translational control of AMPA receptor GluR2 mRNA. Embo J *25*, 4865-4876.

Kocsis E, Trus BL, Steer CJ, Bisher ME, Steven AC. (1991) Image averaging of flexible fibrous macromolecules: the clathrin triskelion has an elastic proximal segment. J Struct Biol. 107:6-14.

Liu, S. Q., and Cull-Candy, S. G. (2000). Synaptic activity at calcium-permeable AMPA receptors induces a switch in receptor subtype. Nature *405*, 454-458.

Liu, Y., Formisano, L., Savtchouk, I., Takayasu, Y., Szabo, G., Zukin, R. S., and Liu, S. J. (2010). A single fear-inducing stimulus induces a transcription-dependent switch in synaptic AMPAR phenotype. Nat Neurosci *13*, 223-231.

Meijering, Jacob, E.M., Sarria, J-C F., Steiner, P., Hirling, H., Unser, M. (2004) Design and Validation of a Tool for Neurite Tracing and Analysis in Fluorescence Microscopy Images. Cytometry Part A, vol. 58, no. 2, pp. 167-176.

Myoga MH, Beierlein M, Regehr WG. (2009) Somatic spikes regulate dendritic signaling in small neurons in the absence of backpropagating action potentials. J Neurosci. 29:7803-14.

Okubo Y, Sekiya H, Namiki S, Sakamoto H, Iinuma S, Yamasaki M, Watanabe M, Hirose K, Iino M. (2010) Imaging extrasynaptic glutamate dynamics in the brain. Proc Natl Acad Sci U S A. 107:6526-31

Rieubland S, Roth A, Häusser M. (2014) Structured connectivity in cerebellar inhibitory networks. Neuron.81:913-29.

Rozov, A., and Burnashev, N. (1999). Polyamine-dependent facilitation of postsynaptic AMPA receptors counteracts paired-pulse depression. Nature *401*, 594-598.

Savtchouk, I., and Liu, S. J. (2011). Remodeling of synaptic AMPA receptor subtype alters the probability and pattern of action potential firing. J Neurosci *31*, 501-511.

Soler-Llavina GJ, Sabatini BL. (2006) Synapse-specific plasticity and compartmentalized signaling in cerebellar stellate cells. Nat Neurosci. 9:798-806.

Sutton MA, Taylor AM, Ito HT, Pham A, Schuman EM. (2007) Postsynaptic decoding of neural activity: eEF2 as a biochemical sensor coupling miniature synaptic transmission to local protein synthesis. Neuron. 55:648-61

Traynelis SF, Silver RA, Cull-Candy SG. (1993) Estimated conductance of glutamate receptor channels activated during EPSCs at the cerebellar mossy fiber-granule cell synapse. Neuron. 11:279-89.

Wang, X. P., and Cooper, N. G. (2009). Characterization of the transcripts and protein isoforms for cytoplasmic polyadenylation element binding protein-3 (CPEB3) in the mouse retina. BMC Mol Biol *10*, 109.

Table S1. Summary of statistical analysis. Related to Figures1, 3-7; Supplemental Figures 1-8

Fig #	Statistic test	Comparison	*P*	post hoc		
Fig 1B	ANOVA	RI of EPSCs at various distance	*0.00000888*		F	14.96
		14-40 vs 40-60 um	*0.00069*	Tukey	q	5.61
		14-40 vs >60 um	*0.0000395*	Tukey	q	6.86
		40-60 vs >60 um	0.79	Tukey	q	0.92
Fig 1C	Kolmogorov–Smirnov test	Decay time constant of individual EPSCs				
		14-40 um vs 40-60 um	*<0.00001*		D	0.31
		40-60 um vs >60 um	*0.015*		D	0.11
		14-40 um vs >60 um	*<0.00001*		D	0.34
	ANOVA	Decay time of each cells	*0.0034*		F	6.37
		14-40 um vs 40-60 um	*< 0.05*	Tukey		
		14-40 um vs >60 um	*< 0.05*	Tukey		
	ANOVA	EPSC amplitude at -60 mV	*0.036*		F	3.52
		14-40 um vs 40-60 um	*< 0.05*	Tukey		
Fig 1D	unpaired t-test	IEM inhibition %	*0.0053*		t	3.65
Fig 1E	ANOVA	Conductance at 3 locations	*0.00049*		F	12.75
		14-40 um vs 40-60 um	*0.00035*	Tukey	q	6.16
		14-40 vs >60 um	*0.0015*	Tukey	q	5.42
		40-60 um vs >60 um	0.996	Tukey	q	0.12
Fig 3A		TEA+ActD+PTX+KYNA treated				
	unpaired t-test	RI at 14-40 vs 40-60 um	0.57		t	0.58
	Mann-Whitney test	RI at 14-40 vs 40-60 um	0.6		Z	-0.53
	unpaired t-test	EPSC decay, 14-40 vs 40-60 um	0.57			
Fig 3B		TEA+ActD vs ActD				
	Kolmogorov–Smirnov test	EPSC decay time at 14-40 um	0.22		K-S	0.093
	Kolmogorov–Smirnov test	EPSC decay time at 40-60 um	*0.0053*		K-S	0.15
Fig 3C		ActD+PTX+KYNA treated				
	unpaired t-test	RI at 14-40 vs 40-60 um	*0.032*		t	-2.5
	unpaired t-test	EPSC decay, 14-40 vs 40-60 um	*0.024*			
Fig 3D	unpaired t-test	γ at 14-40 vs 40-60 um, TEA	0.227		t	-0.58
Fig 3F	Mann-Whitney test	RI at 14-40, CNTL vs w-CTX	*0.015*		Z	-2.42
Fig 4B	left: ANOVA	RI, CHX treated	0.45		F	0.84

Table S1 (cont).

Fig #	Statistic test	Comparison	P	post hoc		
	right: unpaired t-test	RI at > 40 um, cntl vs CHX	*0.02*		t	2.28
Fig 4E	two way ANOVA	RI of SELEX vs cntl oligo at diff. time points				
		factor A	*1.59E-06*		F	35.43
		factor B	*0.00399*		F	5.48
		A: cntl oligo vs Selex	*9.01E-07*	Tukey	q	8.74
		B: 0-15 min vs 30-60 min	*6.05E-03*	Tukey	q	5.08
		B: 0-15 min vs 60-90 min	*7.26E-04*	Tukey	q	6.20
		B: 15-30 min vs 60-90 min	*0.010*	Tukey	q	4.80
Fig 5B	ANOVA	RI of EPSC, cont, TTX, TTX + CHX, CHX	*1.42E-05*		F	14.40
		Cntl vs TTX	*3.99E-05*	Tukey	q	*8.06*
		TTX vd TTX + Chx	*7.14E-04*	Tukey	q	*6.43*
		Chx vs TTX	*7.74E-04*	Tukey	q	*6.38*
	ANOVA	EPSC amplitude at +40 mV	*3.7E-05*		F	12.66
		Cntl vs TTX	*1.6E-05*	Tukey	q	8.60
		TTX vd TTX + Chx	*0.045*	Tukey	q	3.97
		Chx vs TTX	*0.023*	Tukey	q	4.39
	ANOVA	EPSC amplitude at -60 mV	0.34		F	1.18
Fig 5C	Kolmogorov-Smirnov Test	CPEB3-ir in individual SCs; Cntl vs TTX	*9.76E-09*		D	0.40
	Kolmogorov-Smirnov Test	CPEB3 ir in individual GCs, cntl vs TTX	0.89		D	0.086
	Right: ANOVA	CPEB3-ir, cntl vs TTX in SCs and GCs	*0.0017*		F	49.58
		Cntl SC vs TTX SC	*0.0041*	Tukey	t	8.43
		Cntl SC vs Cntl GC	*1.59E-04*	Tukey	t	15.22
		Cntl GC vs TTX GC	0.94695	Tukey	t	0.76
Fig 6C	One-way ANOVA	CPEB3-ir, PTX+KYNA (Control)	*0.035*		F	3.59
		Proximal vs intermediate	0.114	Tukey	q	2.88
		Proximal vs distal	*0.047*	Tukey	q	3.46
		CPEB3-ir, w-CTX	0.86		F	0.04
Fig 6D	Repeated measures ANOVA	CPEB3-ir, ActD	*0.002*		F	10.02
		Proximal vs intermediate	*0.002*	Tukey		5.81
		Proximal vs distal	*0.02*	Tukey		4.32
		actD + TEA	0.055		F	3.46

Fig #	Statistic test	Comparison	*P*	post hoc		
	Wilcoxon signed rank test	Change in CPEB3 at 40-60, ActD+TEA	*0.025*		Z	-2.24
		Change in CPEB3 at 40-60, ActD	0.51		Z	-0.67
Fig 6F	Middle: paired Wilcoxon signed-rank test	GluR2-ir at 14-40 vs 40-140 um	0.0036		Z	-2.91
Fig7C	ANOVA	Membrane PKC-ir	*0.00063*		F	9.51
		CTRL VS TTX	*0.0089*	Tukey	q	5.73
		CTRL VS TTX+PMA	0.97	Tukey	q	0.88
		CTRL VS PMA	0.95	Tukey	q	1.05
		CTRL VS CHE	0.089	Tukey	q	3.95
		TTX VS TTX+PMA	*0.0029*	Tukey	q	6.61
	ANOVA	Cytoplasm PKC-ir	*0.0011*		F	8.38
		CTRL VS TTX	*0.019*	Tukey	q	5.14
		CTRL VS TTX+PMA	0.99	Tukey	q	0.61
		CTRL VS PMA	0.84	Tukey	q	1.44
		CTRL VS CHE	0.11	Tukey	q	3.81
		TTX VS TTX+PMA	*0.0087*	Tukey	q	5.74
	ANOVA	Ratio M/C (PKC-ir)	*1.15E-03*		F	8.38
		CTRL VS TTX	*0.020*	Tukey	q	5.10
		CTRL VS TTX+PMA	0.88	Tukey	q	1.32
		CTRL VS PMA	0.92	Tukey	q	1.17
		CTRL VS CHE	0.097	Tukey	q	3.88
		TTX VS TTX+PMA	*0.0035*	Tukey	q	6.42
		TTX VS PMA	*0.0044*	Tukey	q	6.27
		PMA vs TTX + PMA	1.0	Tukey	q	0.16
		Cntl vs Che	0.16	Tukey	q	3.48
Fig 7D	Repeated measures ANOVA	CPEB3-ir	*0.010*		F	9.66
		Cntl vs CHE	*0.043*	Tukey	t	5105
		Cntl vs PMA	0.96	Tukey	t	0.70
		Cntl vs TTX+CHE	*0.018*	Tukey	t	6.2
		ChE vs TTX + CHE	0.86	Tukey	t	1.11
		TTX+CHE vs PMA	*0.031*	Tukey	t	5.51
	Middle: Repeated measures ANOVA	CPEB3-ir	*0.018*		F	13.12
		Cntl vs TTX	*0.021*	Tukey	t	6.53
		Cntl vs TTX+PMA	0.91	Tukey	t	0.58

Fig #	Statistic test	Comparison	*P*	post hoc		
		TTX vs TTX + PMA	*0.029*	Tukey	t-value	5.97
	Right: ANOVA	% change in CPEB3-ir	*0.00021*	Tukey	F	7.6
		TTX vs PMA	*0.0015*	Tukey	q	6.47
		PMA vs CHE	*0.013*	Tukey	q	5.2
		TTX vs TTX+PMA	*0.033*	Tukey	q	4.64
		PMA vs BIS	*0.030*	Tukey	q	4.70
	One sample t-test	TTX	*0.00001*		t	-8.42
		CHE	*0.017*		t	-4.81
		BIS	*0.0048*		t	-7.58
		TTX+CHE	*0.0083*		t	-10.91
		PMA	0.99		t	-0.02
		PMA + TTX	0.68		t	-0.48
sF1A	Unpaired t-test	Control RI of EPSC at <14 um vs 14-40 um	*0.03*		t	3.08
	Kolmogorov-Smirnov Test	RI of EPSC at <14 um vs 14-40 um	*0.000627*		D	0.66
sF1B	ANOVA	RI w vs w/o spermine at 14-40, >40 um	*0*		F	80.6
		sp >40 vs sp 14-40 um	*6.7E-05*		q	6.75
		no sp 14-40 vs sp 14-40	*8.9E-09*		q	18.0
		no sp>40 vs sp >40 um	*0*		q	11.55
		no sp >40 vs no sp 14-40	0.93		q	0.87
	2 way ANOVA	Distance	0.089		F	2.99
		Treatment	0		F	215.6
		Interaction	0.0066		F	7.92
		40-60 um vs 14-40 um	6.1E-04		q	5.11
		No spermine vs spermine	2.5E-08		q	20.91
sF 4B	Two way ANOVA	EPSC amplitude, actD vs actD+TEA				
		factor A: incubation conditions	0.52		F	0.43
		factor B: distance	0.92		F	0.01
		A x B	0.073		F	3.48
sF 4C	unpaired t-test	Paired pulse ratio at 14-40 vs >40 um	0.78		t	-0.282
	ANOVA	Failure rate at 14-40 and >40um	0.45		F	0.89
		factor B: distance	0.053		F	3.07
		A x B	0.67		F	0.40

Fig #	Statistic test	Comparison	P	post hoc		
		Distance 14-40 vs 40 um	<0.05	Tukey		
sF 4E	one way ANOVA	Changes in RIs	**0.0035**		F	7.03
		Selex vs cntl oligo	**0.0072**	Tukey	q	5.49
		Selex vs Selex+anisomycin	**0.016**	Tukey	q	4.93
		Selex vs anisomycin	**0.020**	Tukey	q	4.75
	one way ANOVA	Initial RI	**0.024**		F	4.23
		Selex+ ani vs cntl oligo	**0.028**	Tukey	q	4.50
sF 5A	Kolmogorov-Smirnov Test	Decay time of EPSCs, cntl vs TTX	**0.0016**		K-S	0.15
sF 5D	ANOVA	RI of EPSCs	**0.00022**		F	7.89
		Cntl vs TTX	**< 0.05**	Tukey		
		TTX vs TTX + Ani	**< 0.05**	Tukey		
	ANOVA	EPSC amplitude at +40 mV	**0.00001**		F	11.6
		Cntl vs TTX	**< 0.05**	Tukey		
		TTX vs TTX + Ani	**< 0.05**	Tukey		
		TTX vs TTX + ActD	**< 0.05**	Tukey		
	ANOVA	EPSC amplitude at -60 mV	0.39		F	1.07
sF 6B	unpaired t-test	Control vs TTX:				
		RI (ratio at +40/60 mV, times 1.5)	**0.023**			-2.80
		EPSC amplitude at -60 mV	0.395			-0.898
		EPSC amplitude at +40 mV	**0.015**			-3.09
sF 7A	Kolmogorov-Smirnov Test	Distribution of CPEB3 ir after shRNA				
		CTRL vs SH1	**5.8E-05**		K-S	0.29
		CTRL vs SH2	**1.4E-04**		K-S	0.223
		CTRL vs LUCI	**0.0039**		K-S	0.218
sF 7B	Kolmogorov-Smirnov Test	CPEB3 ir, with vs w/o PTX+KYNA treatment	0.88		K-S	0.12
sF 7C	Kolmogorov-Smirnov Test	Distribution of p-eEF2 ir in individual stellate cells				
		CTRL vs TTX	**0.011**		K-S	0.15
		CTRL vs NH125	**1.2E-07**		K-S	0.35
	Repeated measures ANOVA	peEF2 ir, cntl, TTX, NH125	0.052		F	6.81
	One sample t-test	CTRL vs TTX	0.85		t	-0.22
		CTRL vs NH125	**0.018**		t	-7.36

Fig #	Statistic test	Comparison	*P*	post hoc	
sF 7E	ANOVA	Membrane thickness	0.85	F	0.33
sF 7G	Kolmogorov–Smirnov test	Distribution of CPEB3 ir			
		CTRL VS TTX	0.00031	K-S	0.13
		CTRL VS CHE	4.8E-07	K-S	0.24
		CTRL VS BIS	0.0046	K-S	0.15
		CTRL VS TTX+CHE	5.3E-09	K-S	0.29
		CTRL VS PMA	0.23	K-S	0.071
		CTRL VS TTX+PMA	0.88	K-S	0.057